JOURNAL OF GEOPHYSICAL RESEARCH: SPACE PHYSICS, VOL. 118, 5149–5156, doi:10.1002/jgra.50501, 2013

Similarities and differences in low- to middle-latitude geomagnetic indices

R. M. Katus[1] and M. W. Liemohn[1]

Received 20 December 2012; revised 19 July 2013; accepted 8 August 2013; published 29 August 2013.

[1] Several versions of low- to middle-latitude geomagnetic indices are examined throughout a 24 year interval and during storm time with respect to a normalized epoch timeline based on several key storm features. In particular, we conduct a quantitative comparison of the storm time superpositioning of the *Dst*, *SYM-H*, and 1 min U.S. Geological Survey *Dst* indices using error analysis and employing descriptive statistics to assess the similarities and differences between them. The events are then categorized by storm intensity and examined as a function of the storm phase. While the indices are highly correlated with each other, dramatic deviation between the indices exists at certain storm epoch times. In particular, the error increases at storm peak and especially for more intense storms. The differences at storm peak are, on average, 20% of the peak value of the indices. These differences arise from the choice of magnetometer stations to include in each index and the various methodologies used to compile the individual perturbation measurements into a global value. The conclusions are that multiple indices should be considered when determining low- to middle-latitude magnetic perturbations and that the difference between the indices should be considered as an error estimate on these values.

Citation: Katus, R. M., and M. W. Liemohn (2013), Similarities and differences in low- to middle-latitude geomagnetic indices, *J. Geophys. Res. Space Physics*, *118*, 5149–5156, doi:10.1002/jgra.50501.

1. Introduction

[2] Geomagnetic disturbances are caused by the interaction between the solar wind and terrestrial magnetosphere (see *Dungey* [1961] and the reviews by *Gonzalez et al.* [1994, 1999]). Geomagnetic activity can be described using ground-based magnetic field observations [e.g., *Mayaud*, 1980]. These measurements are used to calculate several magnetic indices, which explain the near-Earth space currents and allow the study of geomagnetic storms. For instance, *Clauer and McPherron* [1980] found that the magnitude of the partial ring current, as seen in low- to middle-latitude ground-based stations, does not correlate well with the timing of substorm expansion phase onset, usually developing prior to onset. Similarly, *Chen et al.* [1982] conducted numerical simulations and compared the modeled magnetic perturbations to ground-based magnetometer data for a substorm event, concluding that the observed local time asymmetry is due to high-latitude current influences rather than a partial ring current in near-Earth space. A third example is the study by *Iyemori* [1990], who analyzed the local time asymmetries of low- to middle-latitude magnetic perturbations, revealing that the *H*-component asymmetry shifts to earlier local times throughout the main phase of the storm. New indices are continuously being created from ground-based low- to middle-latitude magnetometer data, such as the *Wp* substorm index [*Nosé et al.*, 2012]. While there are many regional and global indices compiled from ground-based magnetometer data, there are few indices that are particularly useful for magnetic storm physics, specifically the hourly *Dst* index and its 1 min counterparts, *SYM-H* and U.S. Geological Survey (USGS) *Dst*.

[3] The disturbance storm time index, *Dst*, describes the progression and intensity of geomagnetic activity. The *Dst* index was developed by *Sugiura* [1964] and is available on the Kyoto World Data Center website. *Dst* uses four ground-based magnetic field observations to characterize deviations from the quiet time horizontal magnetic field (*H*) during a disturbance. The observatories were chosen based on the condition of the measurements and their locations, which are listed in Table 1. The station locations were required to be sufficiently distant from auroral and equatorial electrojets while remaining distributed as evenly as possible in longitude.

[4] The derivation of *Dst* is described in *Mayaud* [1980] and in *Sugiura and Kamei* [1991]. The baseline magnetic perturbation is defined by a power series in time:

$$H_{\mathrm{base}}(\mathrm{T}) = \mathrm{Ar}^2 + \mathrm{Br} + \mathrm{C}$$

In this expression, T is the universal time and r is time in years from a reference epoch time. The coefficients in this expression (A, B, and C) are determined up to the quadratic

[1]Department of Atmospheric, Oceanic and Space Sciences, University of Michigan, Ann Arbor, Michigan, USA.

Corresponding author: R. M. Katus, Department of Atmospheric, Oceanic and Space Sciences, University of Michigan, Space Research Bldg., 2455 Hayward St., Ann Arbor, MI 48109-2143, USA. (rkatus@umich.edu)

2169-9380/13/10.1002/jgra.50501

Table 1. *Dst* Observatory Geomagnetic Coordinates

Observatory	Longitude (E)	Latitude (N)
Hermanus	84°	33°
Kakioka	208°	27°
Honolulu	270°	21°
San Juan	6°	28°

term and are found using the method of least squares on the annual mean values of the five quietest days of the current year and the four preceding years. The baseline values for the adjacent years are calculated by different polynomials. This method may introduce a discontinuity. To minimize the discontinuity, the baseline value at the end of the current year is included as an additional data point in the polynomial fitting. For a more detailed description of the process, see *Mayaud* [1980] and *Sugiura and Kamei* [1991].

[5] The solar quiet daily variation, *Sq*, is determined for each observatory by a double Fourier series as a function of local time (t) and month (s):

$$S_q(\mathrm{t},\mathrm{s}) = \sum_\mathrm{m}\sum_\mathrm{n} \mathrm{A_{mn}} \cos(\mathrm{mt} + \alpha_\mathrm{m}) \cos(\mathrm{ns} + \beta_\mathrm{n})$$

In this expression, m and n are the order of the Fourier expansion, and $\mathrm{A_{mn}}$, α_m, and β_n are the corresponding Fourier coefficients. The coefficients of the *Sq* variation are calculated from the geomagnetic field data for the five quietest days of the month. These quietest days are determined in UT. That is, the five local days that have the maximum overlap with the five quietest UT days are used to define the average *Sq* variation for the local day at each observatory. The variation in *Dst* caused by the noncyclic change is removed from the *Sq* current using the hourly values calculated for the local days before and after the 5 days selected.

[6] The disturbance variation, $D(\mathrm{T})$, for each observatory is defined as what is left after the baseline value and the *Sq* variation are removed from the observation.

$$D(\mathrm{T}) = H_{\mathrm{obs}} – H_{\mathrm{base}}(\mathrm{T}) – Sq(\mathrm{T})$$

Dst is then defined as the four-observatory average of the disturbance field normalized to the dipole equator.

$$Dst(\mathrm{T}) = < D(\mathrm{T}) > / < \cos\theta >$$

The normalization uses the average of the cosines of each observatory's dipole latitude. The normalization to the dipole equator minimizes the undesired effect from missing hourly values. *Mayaud* [1980] showed that the latitudinal normalization minimizes local time residual effects.

[7] Although *Dst* is one of the most important data sets in space weather, it still has several issues [e.g., *Clauer et al*., 1980]. They estimated that the quiet time random error in low- to middle-latitude perturbations is typically about ±6 nT, resulting from uncertainties in the *Sq* current system. *Friedrich et al*. [1999] and *Munsami* [2000] quantified the contribution of the substorm current wedge to the *Dst* index, which can be as large as 40 nT if the stations are aligned in a certain way relative to the auroral electrojet. Two more examples are given in *Mursula et al*. [2008]. First, they argue that the disturbance field at each station should be normalized by the cosine of the geomagnetic latitude before being averaged to produce *Dst*. They showed that averaging first causes a bias in the contribution to variation based on latitude. *Mursula et al*. [2008] also discussed correcting the quiet time seasonal variation.

[8] Another issue with the *Dst* index is that the resolution is insufficient for describing effects that occur with time scales of less than 1 h. One method to remedy the low time resolution is the use of high time resolution data (1 min or 1 s). These data are now available for all four *Dst* stations. While these data should be used to calculate the high-resolution *Dst* in the modern era, they do not help with historic data. Another method to remedy the low time resolution would be to utilize additional magnetometer stations [see, e.g., *Clauer et al*., 2003].

[9] The *SYM-H* index describes the geomagnetic disturbance field at midlatitudes with a 1 min resolution [*Iyemori*, 1990; *Iyemori et al*., 1992]. *SYM-H* is calculated from 6 of the 10 possible observatories listed in Table 2. The observatories used each month depend upon the availability and the quality of the observations. Like *Dst*, *SYM-H* removes the baseline and *Sq* field to calculate the disturbance field. Next, *SYM-H* performs a transformation from a geomagnetic to a dipole coordinate system. Then the six stations are averaged.

[10] While *Dst* and *SYM-H* are argued to be essentially the same [e.g., *Sugiura and Poros*, 1971], they are inherently different. One reason for the difference is the midlatitude observatories included in the calculation of *SYM-H*, but not *Dst* [*Iyemori*, 1990]. Magnetic disturbances vary with latitude [*Araki et al*., 1997] and with proximity to local current systems, which implies that *SYM-H* will reflect variation caused by different processes. Another reason for the difference between *Dst* and *SYM-H* arises in the processing methodologies to compile the index values.

[11] The United States Geological Survey also produces a 1 min low-latitude disturbance index [*Gannon and Love*, 2011], which we will refer to as the USGS index. The USGS index uses the same four low-latitude observatories as *Dst*. USGS is calculated using the time and frequency space method described in *Love and Gannon* [2009]. They showed that the main field data reveal several sets of harmonics, which they used to remove the *Sq* variation.

Table 2. *SYM-H* Observatory Geomagnetic Coordinates

Observatory	Longitude (E)	Latitude (N)
San Juan	6°	28°
Fredericksburg	353°	48°
Boulder	321°	48°
Tucson	316°	39°
Honolulu	270°	21°
Memambetsu	211°	35°
Alibag	146°	10°
Martin de Vivies	144°	-46°
Hermanus	84°	33°
Chambon-la-Foret	85°	49°

Table 3. Descriptive Statistics for the Entire 1985 Through 2009 Interval

	Mean	Median	Standard Deviation	Min	Max	R[a]	RMSE[a]
Dst	−16.8	−12	22.97	−589	81	0.93	9.1
SYM-H	−14.5	−10	22.82	−720	149	0.93	11.0
USGS	−7.3	−3.9	21.3	−524.4	132.3	0.95	12.1

[a]Comparisons are made with the index below it in the table, cycling back to the top for the last row's values.

[12] Although the differences between the calculational methodologies of the *Dst*, *SYM-H*, and USGS indices are well documented [e.g., *Sugiura*, 1964; *Iyemori*, 1990; *Iyemori et al*., 1992; *Love and Gannon*, 2009; *Gannon and Love*, 2011], the indices are often used interchangeably in both data analysis studies [e.g., *Ohtani et al*., 2001; *Nosé et al*., 2003; *Reeves et al*., 2003] and data-model comparisons [e.g., *Fok et al*., 2003, 2011; *Jordanova et al*., 2006; *Liemohn et al*., 2007; *Zhang et al*., 2007]. *Wanliss and Showalter* [2006] conducted statistics on the similarity of the *SYM-H* and *Dst* indices, showing that the correlation between them is very high (above 0.9) with differences of only 10 or 20 nT during storms and concluding that *SYM-H* can be used as a high-resolution version of *Dst*. This study builds on the results of *Wanliss and Showalter* [2006], examining the validity of the interchangeability of these indices by investigating the similarities and differences in the *Dst*, *SYM-H*, and USGS indices. We begin with an inspection of the complete interval in which the indices' availability overlaps. We then conduct a storm-based analysis. While we verify that during quiet times up to moderate storm activity the indices are all strongly correlated, we also find that the relationship between the indices is dependent on storm time phase and intensity.

2. Data

[13] This study begins with the full interval in which the *Dst*, *SYM-H*, and USGS indices' availability overlaps (1985 through 2009). Throughout the interval, the temporal resolution is 1 min for *SYM-H* and USGS but 1 h for *Dst*. To conduct a one-to-one comparison of data with different time resolutions, *Dst* values are assumed to be constant along each hour. That is, each minute value is set as the corresponding hour value.

[14] An initial overview of the data is described in Table 3. The mean and median *Dst* (−16.8 and −12 nT) are more negative than *SYM-H* (−14.5 and −10 nT) or USGS (−7.3 and −3.9 nT). The range in *SYM-H* (−720 nT, 149 nT) is much larger than *Dst* (−589 nT, 81 nT) or USGS (−524.4 nT, 132 nT). While the ranges show that the 24 year interval contains super storms, the standard deviation reveals that the vast majority of the interval is quiet time data. That is, at least 95% of the data are greater than −40 nT in all three indices.

[15] The correlation coefficient (R) and root-mean-square error (RMSE) values in Table 3 are comparisons for each index with the index below it in the table, with the value in the USGS line being with *Dst*. Table 3 verifies that the correlation between any two of the indices is large (R of at least 0.93). The RMSE values are all below 13 nT. These values are in complete agreement with *Wanliss and Showalter* [2006]. The large correlations and small RMSE values may be interpreted as a validation that the indices are essentially the same, but this initial overview does not tell the whole story, as will be investigated below.

[16] Figure 1 presents the three indices during two example storms. In both examples, the indices all show a similar trend, consistent with the high correlation. In the 14 October 2002 storm, *Dst* shows an offset of about 20 nT throughout the event compared to the other two indices. This offset is consistent with the lower mean and median of *Dst* seen in Table 3. Additionally, the 3 April 2004 storm reveals differences greater than 40 nT between the indices around the peak (and differences of 20 nT elsewhere in the time series). These types and magnitudes of difference are common during intense storm intervals and reveal underlying systemic variation between the indices. Such dramatic differences will have implications when these values are used to interpret the physics of magnetic storms, and therefore, below, we present a systematic examination of these disparities.

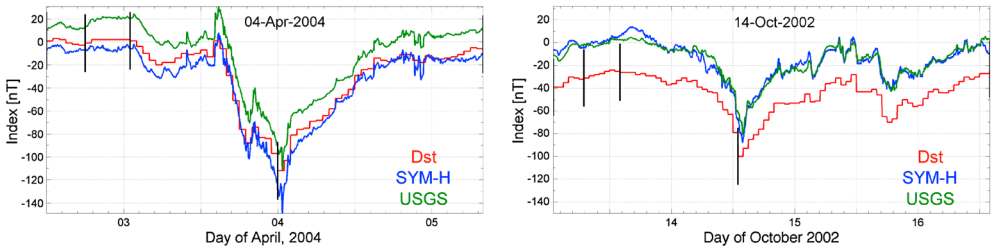

Figure 1. *Dst*, *SYM-H*, and USGS time series for two example storms, (left) 3 April 2004 and (right) 14 October 2002. The black vertical lines, extending ±25 nT from *Dst*, indicate the start of the initial phase (SSC not required), the beginning of the main phase, the peak, and the end of the recovery phase (along the right edge of the plots).

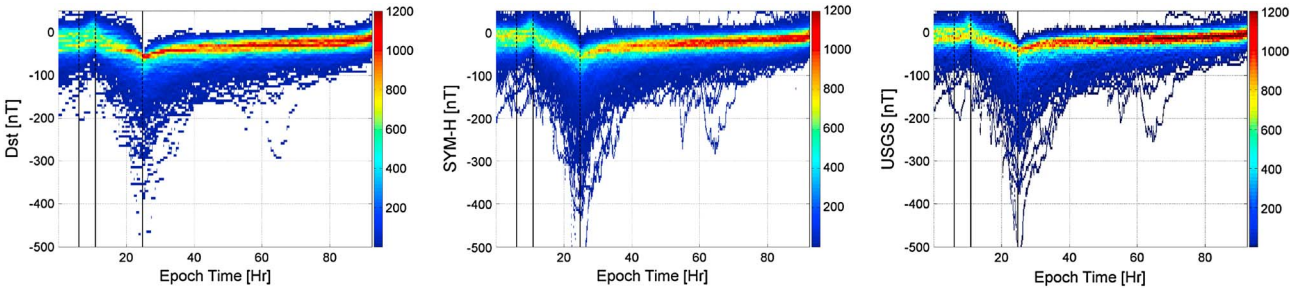

Figure 2. *Dst*, *SYM-H*, and USGS occurrence rate density superposed along the normalized epoch timeline for all storms meeting the selection criteria. The black vertical lines show the storm sudden commencement (not required), beginning of the main phase, storm peak, and end of recovery phase markers used to normalize the timeline.

3. Storms

[17] To progress from a whole-interval-based examination to a storm-based statistical analysis, this study parses the 24 year interval using an automated procedure similar to that of *Katus et al*. [2013]. The first step in the storm-finding procedure searches for negative peaks in *Dst* of less than −50 nT. The second step finds the maximum value within the 24 h prior to the peak and 96 h following the peak. These times mark the beginning of the main phase and the end of the recovery phase, respectively. The third step looks for a sharp increase in *Dst* prior to the start of the main phase corresponding to the storm sudden commencement (SSC). *Katus et al*. [2013] defined the SSC by an increase of at least 10 nT in *Dst* within 8 h before the beginning of the main phase. Unlike *Katus et al*. [2013], this study does not require a SSC or an extended period of quiet time prior to each event, allowing the inclusion of 697 events. Requiring an SSC would have reduced this number to approximately 293 events. The epoch markers are shown as the black vertical lines extending ±25 nT from *Dst* for the example storms given in Figure 1.

[18] The storm phase markers and the average duration of each phase were then used to create a normalized epoch timeline similar to *Katus et al*. [2013]. This is useful because *Ilie et al*. [2008] showed that using a single reference time during storms only resolves features within a few hours surrounding the chosen epoch time. Outside of this window, the different lengths of the phases for individual storms cause the time-specific features of the data to be lessened. *Katus et al*. [2013] showed that a normalized epoch timeline, using multiple references throughout the storm sequence, minimizes the error between the superposed averaged *Dst* time series and the event-specific *Dst* time series (compared to using only a single reference time).

[19] For each storm interval, the duration of each phase was expanded or contracted to match the average length of that storm phase, and the values were then interpolated onto a 1 min cadence within this standardized phase duration. Note that the data are interpolated in time within each storm phase so that the beginning to ending match the average length for that phase. The normalized timeline provides a base to superpose the *Dst*, *SYM-H*, and USGS storm data in Figure 2. The storm sudden commencement, beginning of the main phase, storm peak, and end of the recovery phase markers are shown as black vertical lines in each of the three plots in the figure. Note that the end of the recovery phase is also the end of the plot. The color scale describes the histogram count of data points at that epoch time and magnitude.

[20] Examination of Figure 2 reveals a strong correlation in the form of a similar trend in all three indices. The high density of data near the storm peak shows that most of the storms can be categorized as moderate events (peak *Dst* between −50 and −100 nT). The spread of the density near the peak then shows the remaining intense events (peak *Dst* of −100 nT or less).

[21] There are a couple of noteworthy differences between the plots in Figure 2. Although the plot axes are trimmed (not showing the most extremes), the true range in storm time *SYM-H* is much larger than that in either *Dst* or USGS (as seen in Table 3). In addition, even though USGS is also a 1 min cadence index, *SYM-H* shows larger short-time-scale variations than either of the other two indices. This can also be seen in the example storm intervals presented in Figure 1 by examining the quick variation in *SYM-H*. Another point to mention about Figure 2 is that the mean USGS along the epoch time line is closer to zero than the other two indices. The smaller mean is consistent with the mean for all data in Table 3 and the example storms in Figure 1.

[22] The scatterplots in Figure 3 describes the relationship between the storm time *Dst*, *SYM-H*, and USGS. The color scale defines the histogram count at each magnitude bin. The red line and annotation define the best fit line, and the black line describes the one-to-one line. It should be noted that the axes in these plots are artificially limited. This is done so that the range does not prohibit viewing the key details. The data outside of the range are shown as the histogram count along the border of each plot (particularly *SYM-H*). Note, however, that the actual index values are used in the statistical calculations discussed below. Each plot shows that the indices are all well correlated during storm time. That is, the data are tightly aligned with the reference line. The best fit lines show the difference between the one-to-one line (perfect correlation) and the best fit polynomial. The polynomial also shows the systematic offset for each pair of indices. In addition to the linear fit function, the RMSE between any two of the three indices is given on each plot. The largest RMSE is between *Dst* and USGS (16 nT). The RMSE values follow the offset seen in the previous plots

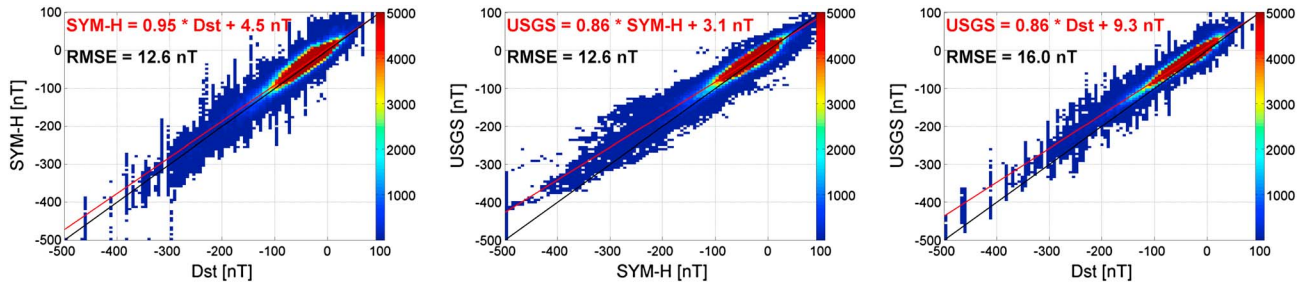

Figure 3. The distribution of storm time *Dst*, *SYM-H*, and USGS indices compared against each other in a one-to-one scatterplot comparison. The one-to-one line is shown in black and the best fit line and equation in red. The sum of all data outside of the axis range is shown on the border.

and the difference in the mean seen in Table 3. While the RMSE values are strongly influenced by the large amount of data near zero (the big red spots on each plot), the results do not follow the ordering in highest correlation seen in Table 3 for the entire 24 year interval.

[23] To further examine the relationship between the *Dst*, *SYM-H*, and USGS indices with respect to their dependence on storm intensity, it is useful to subdivide the storm intervals into different categories. Binning the events by magnitude produced the following breakdown: 518 moderate storms ($-50\,\mathrm{nT} <$ peak $Dst < 100\,\mathrm{nT}$), 137 intense storms ($-100\,\mathrm{nT} <$ peak $Dst < -200\,\mathrm{nT}$), and 27 super storms ($-200\,\mathrm{nT} <$ peak Dst). These bin sizes allowed a relatively large number of events in each group.

[24] Figure 4 describes the histogram count of the difference between each index along the normalized epoch timeline for storms separated as moderate, intense, or super storms. The RMSE between each set of indices is also given on each plot. There are several striking features in each plot of Figure 4. The data in all of the plots tend to

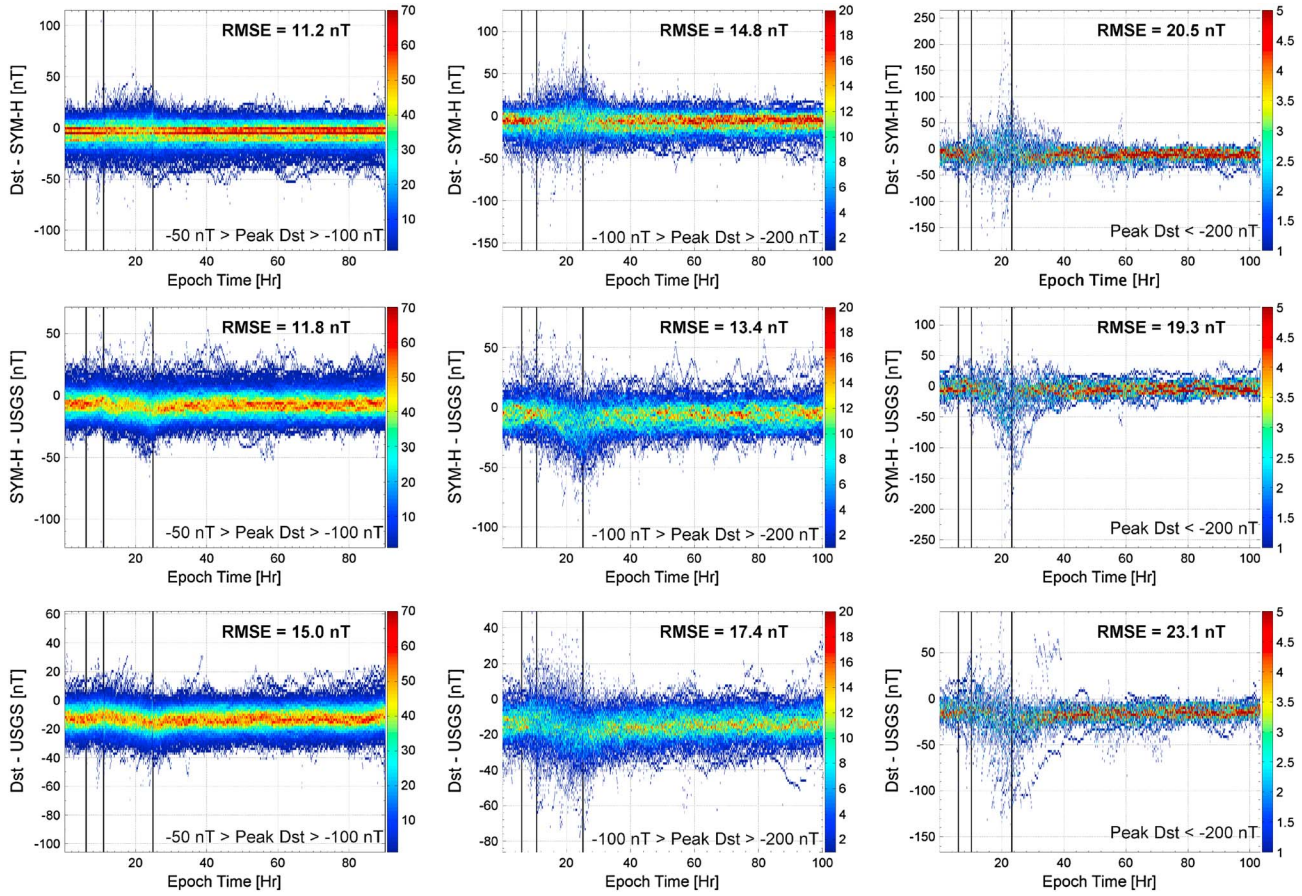

Figure 4. The distribution of the difference between each pair of indices, along the normalized superposed epoch timeline for (left) moderate, (middle) intense, and (right) super storms. Note that the scales are different.

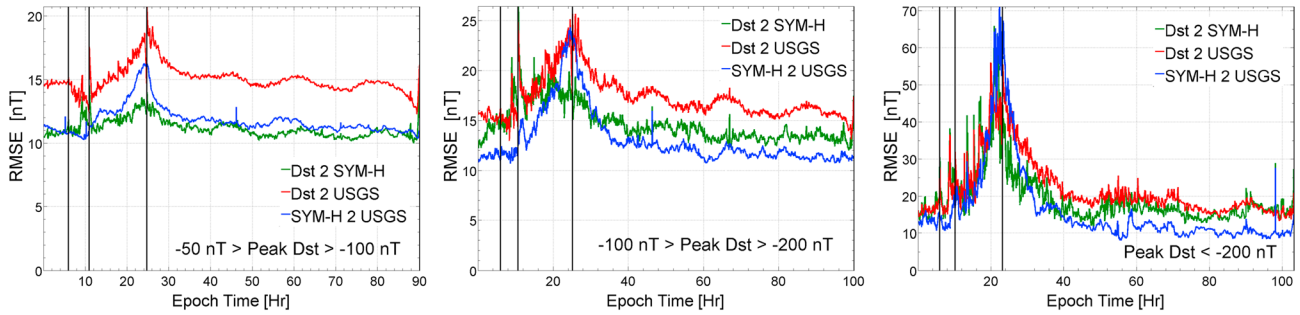

Figure 5. The RMSE, along the normalized superposed epoch timeline for (left) moderate, (middle) intense, and (right) super storms. Note that the scales are different.

be negative. This negative trend implies a systematic offset with *Dst* having the largest negative values and USGS being closest to zero. The trend holds throughout epoch time in all three storm magnitude bins. The spread in the distribution of the data in all of the plots shows that the difference grows approaching the storm peak. Noticing the different scales among the panels in Figure 4, the RMSE reveals that the difference grows proportionally to the magnitude of the storm.

[25] To further investigate this systematic difference between the indices, Figure 5 shows the RMSE between the indices as a function of epoch time for each storm size category. Each plot shows a systematic RMSE of at least 10 nT along the entire timeline. The RMSE grows approaching the storm peak, and the growth is proportional to the magnitude of the storm intensity. Apart from a few short-lived spikes, the largest RMSE values occur in the late main phase and early recovery phase, within 2 h of the storm peak (on the normalized timeline scaled to the average phase length for each intensity category), and range from 13 to 23 nT for the moderate storm intervals, 20 to 26 nT for the intense storms, and 55 to 70 nT for the super storms. Therefore, the ratio of the RMSE to the mean *Dst* at storm peak for each of the storm magnitude bins is near 0.2 for all three of the storm intensity categories. The differences are smallest between *Dst* and *SYM-H* (the green curves in the panels of Figure 5), while the differences of both of these with the USGS index are systematically larger in the late main phase and near storm peak.

[26] The short-lived spikes in the RMSE time series are very interesting because these are most likely erroneous values in the indices. Times with large jumps were found in both the *SYM-H* and USGS data sets, lasting a single data value or sometimes several values together, with jumps back to the previous index level immediately afterward. They look like bad data points, but they were intentionally left in this analysis because they exist in the research grade index values available to the community. These RMSE spikes illustrate the points that a single index for storm intensity is problematic and that multiple indices should be considered when conducting an analysis of storms.

4. Discussion and Conclusion

[27] There are several distinctions in the calculation of *Dst*, *SYM-H*, and USGS that may cause inconsistent variation. First, each index applies different methods to remove irrelevant fluctuations and normalize to the equator. Second, the averaging in *Dst* results in the loss of fluctuations with time scales of less than 1 h. Third, the use of higher-latitude stations in *SYM-H* may contaminate the data with fluctuations caused by polar currents.

[28] This study finds that the three indices are not the same. *SYM-H* has a larger range than the other two indices. The difference between the indices increases during times of geomagnetic activity. The difference grows approaching the peak of a storm and is proportional to the intensity of the storm. Comparing the RMSE and mean peak magnitude reveals an error of approximately 20% between the indices at the peak of the storm. In addition, short-lived spikes in the RMSE time series reveal that the available indices sometimes include erroneous values.

[29] There are a few reasons why the differences between the indices should be expected. The quiet time and *Sq* variation subtraction is different between the *Dst*, *SYM-H*, and USGS. Because these offsets are functions of both local time and universal time, these subtractions not only introduce a baseline offset between the indices but also can lead to storm epoch time-dependent variations. This is especially true for the *SYM-H* index, for which different stations are included each month. Another reason for the difference is that the *SYM-H* index includes additional stations at higher magnetic latitudes than *Dst* or USGS. This means that auroral zone ionospheric currents could be a larger factor in these magnetometer measurements, introducing additional variability to the *SYM-H* index. In addition, the USGS index uses a different method for averaging the disturbance signals from the stations, introducing another reason why the indices could be different. The analysis presented above does not attempt to rank the indices or determine which method is best; rather, it focuses on identifying the similarities and differences between them, especially during magnetic storm intervals.

[30] The indices are often used to test models of the inner magnetosphere [e.g., *Jordanova et al.*, 1998, 2001; *Liemohn et al.*, 1999, 2001; *Ebihara and Ejiri*, 2000; *Fok et al.*, 2003; *Chen et al.*, 2003; *Clauer et al.*, 2003]. In fact, the recent full-solar-cycle data-model comparison studies of magnetic storms characterizing the influence of different storm drivers [*Liemohn and Jazowski*, 2008; *Liemohn et al.*, 2010; *Liemohn and*

Katus, 2012] all included model assessments against *Dst* and/or *SYM-H* as a major component of the analysis. These tests demonstrate knowledge of the physical processes governing inner magnetospheric dynamics and the ability to replicate and understand these processes. If one index was accepted to be the correct disturbance index and used consistently, then the difference between the three indices would not matter. The practice of using the indices interchangeably, regardless of the differences in the three indices, may bias test results.

[31] Rather than accepting the potential bias caused by inconsistently choosing to use one of the three indices, all three indices may be used to highlight important features. The values at any time can be used to create a margin of error. The range would provide a universal time-dependent error bar. This error bar may also provide important information similar to that of the asymmetric index (ASY) or implying the importance of high-altitude current systems. These types of relationships should be examined in the future.

[32] **Acknowledgments.** The authors would like to thank NASA and NSF for funding this research through various grants (specifically, from NASA via grants NNX08AQ15G, NNX09AF45G, NNX10AQ34C, and NNX11AO60G and NSF through grants ATM-0802705, ATM-0903596, and AGS-1102863), including a NASA Graduate Student Research Program fellowship from Marshall Space Flight Center (grant NNX10AL32H). The authors would also like to thank the Kyoto World Data Center for providing access to the *Dst* and *SYM-H* indices, and United States Geological Survey for providing access to the USGS 1 min *Dst*.

[33] Robert Lysak thanks Kazue Takahashi and two anonymous reviewers for their assistance in evaluating this paper.

References

Araki, T., et al., (1997), Anomalous sudden commencement on March 24, 1991, *J. Geophys. Res.*, *102*, 14,075–14,086, doi:10.1029/96JA03637.

Chen, C.-K., R. A. Wolf, M. Harel, and J. L. Karty (1982), Theoretical magnetograms based on quantitative simulation of a magnetospheric substorm, *J. Geophys. Res.*, *87*, 6137–6152.

Chen, M. W., M. Schulz, G. Lu, and L. R. Lyons (2003), Quasi-steady drift paths in a model magnetosphere with AMIE electric field: Implications for ring current formation, *J. Geophys. Res.*, *108*(A5), 1180, doi:10.1029/2002JA009584.

Clauer, C. R., and R. L. McPherron (1980), The relative importance of the interplanetary electric field and magnetospheric substorms on partial ring current development, *J. Geophys. Res.*, *85*, 6747–6759.

Clauer, C. R., R. L. McPherron, and M. G. Kivelson (1980), The uncertainty in ring current parameters due to the quiet magnetic field variability at midlatitudes, *J. Geophys. Res.*, *85*, 633–643.

Clauer, C. R., M. W. Liemohn, J. U. Kozyra, and M. L. Reno (2003), The relationship of storms and substorms determined from mid-latitude ground-based magnetic maps, in *Disturbances in Geospace: The Storm-Substorm Relationship*, AGU Monogr. Ser., vol. 142, edited by S. J. Sharma, p. 143, AGU, Washington, D. C.

Dungey, J. W. (1961), Interplanetary magnetic field and the auroral zones, *Phys. Rev. Lett.*, *6*, 47–48.

Ebihara, Y., and M. Ejiri (2000), Simulation study on fundamental properties of the storm-time ring current, *J. Geophys. Res.*, *105*, 15,843–15,859, doi:10.1029/1999JA900493.

Fok, M.-C. et al., (2003), Global ENA image simulations, *Space Sci. Rev.*, *109*, 77–103.

Fok, M.-C., T. E. Moore, S. P. Slinker, J. A. Fedder, D. C. Delcourt, M. Nosé , and S.-H. Chen (2011), Modeling the superstorm in November 2003, *J. Geophys. Res.*, *116*, A00J17, doi:10.1029/2010JA015720.

Friedrich, E., G. Rostoker, M. G. Connors, and R. L. McPherron (1999), Influence of the substorm current wedge on the *Dst* index, *J. Geophys. Res.*, *104*, 4567–4575.

Gannon, J. L., and J. J. Love (2011), USGS 1-min Dst index, *J. Atmos. Sol. Terr. Phys.*, *73*, 323–334, doi:10.1016/j.jastp.2010.02.013.

Gonzalez, W. D., J. A. Joselyn, Y. Kamide, H. W. Kroehl, G. Rostoker, B. T. Tsurutani, and V. M. Vasyliunas (1994), What is a geomagnetic storm?, *J. Geophys. Res.*, *99*, 5771–5792.

Gonzalez, W. D., B. T. Tsurutani, and A. L. Clua de Gonzalez (1999), Interplanetary origin of geomagnetic storms, *Space Sci. Rev.*, *88*, 529–562.

Ilie, R., M. W. Liemohn, M. F. Thomsen, J. E. Borovsky, and J. Zhang (2008), Influence of epoch time selection on the results of superposed epoch analysis using ACE and MPA data, *J. Geophys. Res.*, *113*, A00A14, doi:10.1029/2008JA013241.

Iyemori, T. (1990), Storm-time magnetospheric currents inferred from mid-latitude geomagnetic field variations, *J. Geomagn. Geoelectr.*, *42*(11), 1249–1265.

Iyemori, T., T. Araki, T. Kamei, and M. Takeda (1992). Mid-latitude geomagnetic indices ASY and SYM (provisional) No. 1, 1989, Data Analysis Center for Geomag. and Space Magnetism, Kyoto Univ., Kyoto.

Jordanova, V. K., C. J. Farrugia, J. M. Quinn, R. M. Thorne, K. E. Ogilvie, R. P. Lepping, G. Lu, A. J. Lazarus, M. F. Thomsen, and R. D. Belian (1998), Effect of wave-particle interactions on ring current evolution for January 10–11, 1997: Initial results, *Geophys. Res. Lett.*, *25*, 2971–2974, doi:10.1029/98GL00649.

Jordanova, V. K., C. J. Farrugia, R. M. Thorne, G. V. Khazanov, G. D. Reeves, and M. F. Thomsen (2001), Modeling ring current proton precipitation by electromagnetic ion cyclotron waves during the May 14–16, 1997, storm, *J. Geophys. Res.*, *106*, 7–22, doi:10.1029/2000JA002008.

Jordanova, V. K., Y. S. Miyoshi, S. Zaharia, M. F. Thomsen, G. D. Reeves, D. S. Evans, C. G. Mouikis, and J. F. Fennell (2006), Kinetic simulations of ring current evolution during the Geospace Environment Modeling challenge events, *J. Geophys. Res.*, *111*, A11S10, doi:10.1029/2006JA011644.

Katus, R., M. W. Liemohn, D. L. Gallagher, A. J. Ridley, and S. Zou (2013), Evidence for potential and inductive convection during intense geomagnetic events using normalized superposed epoch analysis, *J. Geophys. Res. Space Physics*, *118*, 181–191, doi:10.1029/2012JA017915.

Liemohn, M. W., and M. Jazowski (2008), Ring current simulations of the 90 intense storms during solar cycle 23, *J. Geophys. Res.*, *113*, A00A17, doi:10.1029/2008JA013466.

Liemohn, M. W., and R. Katus (2012), Is the storm time response of the inner magnetospheric hot ions universally similar or driver dependent?, *J. Geophys. Res.*, *117*, A00L03, doi:10.1029/2011JA017389.

Liemohn, M. W., J. U. Kozyra, V. K. Jordanova, G. V. Khazanov, M. F. Thomsen, and T. E. Cayton (1999), Analysis of early phase ring current recovery mechanisms during geomagnetic storms, *Geophys. Res. Lett.*, *26*, 2845–2848.

Liemohn, M. W., J. U. Kozyra, M. F. Thomsen, J. L. Roeder, G. Lu, J. E. Borovsky, and T. E. Cayton (2001), Dominant role of the asymmetric ring current in producing the stormtime *Dst**, *J. Geophys. Res.*, *106*, 10,883–10,904.

Liemohn, M. W., J. U. Kozyra, A. J. Ridley, M. F. Thomsen, M. G. Henderson, P. C. Brandt, and D. G. Mitchell (2007), Modeling the ring current response to a sawtooth oscillation event, *J. Atmos. Sol. Terr. Phys.*, *69*, 67–76.

Liemohn, M. W., M. Jazowski, J. U. Kozyra, N. Ganushkina, M. F. Thomsen, and J. E. Borovsky (2010), CIR vs. CME drivers of the ring current during intense magnetic storms, *Proc. R. Soc. A*, *466*(2123), 3305–3328, doi:10.1098/rspa.2010.0075.

Love, J. J., and J. L. Gannon (2009), Revised *Dst* and the epicycles of magnetic disturbance: 1958-2007, *Ann. Geophys.*, *27*, 3101–3131.

Mayaud, P. N. (1980), *Derivation, Meaning, and Use of Geomagnetic Indices*, Geophys. Monogr. Ser., vol. 22, 154 pp., AGU, Washington, D. C., doi:10.1029/GM022.

Munsami, V. (2000), Determination of the effects of substorms on the storm-time ring current using neural networks, *J. Geophys. Res.*, *105*, 27,833–27,840.

Mursula, K., L. Holappa, and A. Karinen (2008), Correct normalization of the *Dst* index, *Astrophys. Space Sci. Trans.*, *4*(2), 41–45.

Nosé, M., R. W. McEntire, and S. P. Christon (2003), Change of the plasma sheet ion composition during magnetic storm development observed by the Geotail spacecraft, *J. Geophys. Res.*, *108*(A5), 1201, doi:10.1029/2002JA009660.

Nosé, M., et al., (2012), Wp index: A new substorm index derived from high-resolution geomagnetic field data at low latitude, *Space Weather*, *10*, S08002, doi:10.1029/2012SW000785.

Ohtani, S., M. Nosé, G. Rostoker, H. Singer, A. T. Y. Lui, and M. Nakamura (2001), Storm-substorm relationship: Contribution of the tail current to *Dst*, *J. Geophys. Res.*, *106*, 21,199–21,209, doi:10.1029/2000JA000400.

Reeves, G. D., K. L. McAdams, R. H. W. Friedel, and T. P. O'Brien (2003), Acceleration and loss of relativistic electrons during geomagnetic storms, *Geophys. Res. Lett.*, *30*(10), 1529, doi:10.1029/2002GL016513.

Sugiura, M. (1964), Hourly values of equatorial *Dst* for the IGY, *Ann. Int. Geophys. Year*, *35*, 9–45.

Sugiura, M., and D. J. Poros (1971), Hourly values of equatorial *Dst* for the years 1957 to 1970, GSFC Doc. X-645-71-278, Goddard Space Flight Center, Greenbelt, Md.

Sugiura, M., and T. Kamei (1991), Equatorial *Dst* index 1957-1986, in *IAGA Bull.*, *40*, edited by A. Berthelier and M. Menvielle, ISGI Publ. Off., Saint-Maur-des-Fosse's, France.

Wanliss, J. A., and K. M. Showalter (2006), High-resolution global storm index: *Dst* versus SYM-H, *J. Geophys. Res.*, *111*, A02202, doi:10.1029/2005JA011034.

Zhang, J., et al., (2007), Understanding storm-time ring current development through data-model comparisons of a moderate storm, *J. Geophys. Res.*, *112*, A04208, doi:10.1029/2006JA011846.